Practical Modeling for Wind Load Paths in a Realistic Light-Frame Wood House

Citation	Kathryn S. Pfretzschner, Rakesh Gupta, and Thomas H. Miller (2014). "Practical Modeling for Wind Load Paths in a Realistic Light-Frame Wood House." Journal of Performance of Constructed Facilities, 28(3), 430-439. doi:10.1061/(ASCE) CF.1943-5509.0000448
DOI	10.1061/(ASCE)CF.1943-5509.0000448
Publisher	American Society of Civil Engineers
Version	Accepted Manuscript
Terms of Use	http://cdss.library.oregonstate.edu/sa-termsofuse

PRACTICAL MODELING FOR WIND LOAD PATHS IN A REALISTIC, LIGHT-FRAME WOOD HOUSE

Kathryn S. Pfretzschner[1], Rakesh Gupta[2], M.ASCE and Thomas H. Miller[3], M. ASCE

ABSTRACT

The objective of this study was to develop and validate practical modeling methods for investigating load paths and system behavior in a realistic, light-frame wood structure. The modeling methods were validated against full-scale tests on sub-assemblies and an L-shaped house. The model of the L-shaped house was then modified and used to investigate the effects of re-entrant corners, wall openings and gable-end retrofits on system behavior and load paths. Results from this study showed that the effects of adding re-entrant corners and wall openings on uplift load distributions were dependent on the orientation of the trusses with respect to the walls. Openings added to walls parallel to the trusses had the least effect on loads carried by the remaining walls in the building. Varying re-entrant corner dimensions under ASCE 7-05 (ASCE 2005) design wind loads caused increasing degrees of torsion throughout the house, depending on the relative location and stiffness of the in-plane walls (parallel to the wind loads) as well as the assumed direction of the wind loads. Balancing the stiffness of the walls on either side of the house with the largest re-entrant corner helped to decrease torsion in the structure under lateral loads. Finally, although previous full-scale tests on gable-end sections verified the effectiveness of the gable-end retrofit that was recently adopted into the 2010 Florida building code, questions remained about the effects of the retrofit on torsion in a full building. The current study found that adding the gable-end retrofits to the L-shaped house did not cause additional torsion.

Keywords: structural systems, structural models, residential buildings

---

[1]Former Graduate Research Assistant, Dept. of Wood Sci. & Eng. and School of Civil & Const. Eng., Oregon State University, Corvallis, OR-97331.
[2]Professor, Dept. of Wood Sci. & Eng., Oregon State University, Corvallis, OR-97331.
Corresponding Author: rakesh.gupta@oregonstate.edu
[3]Assoc. Prof., School of Civil & Const. Eng., Oregon State University, Corvallis, OR-97331.

INTRODUCTION

In the United States wind damage accounted for approximately 70 percent of insured losses from 1970 to 1999 (Holmes 2001). Wood-frame residential structures are particularly vulnerable to damage from wind due to their light weight. Additionally, the majority of existing single-family houses in the United States were constructed before building codes were updated after Hurricane Andrew in 1992. More recent wind storms in the United States, including the 2005 hurricane Katrina and the 2011 Joplin, Missouri, and Tuscaloosa, Alabama, tornadoes have shown that structural damage from wind is still a prevalent issue, especially for wood-framed residential structures. Structural investigations from these hurricane and tornado events showed that the main source of damage in houses was an overall lack of design for uplift load paths (van de Lindt et al. 2007 and Prevatt et al. 2012a). Additionally, gable-end failures were reported as an area of concern (van de Lindt et al. 2007 and Prevatt et al. 2012a). In order to develop retrofitting options and improve building codes for residential structures, it is necessary to gain a better understanding of system behavior and load paths in light-frame structures.

Analyzing system behavior in complex structures requires the development of practical and accurate analytical models validated against full-scale tests. Phillips et al. (1993) and Paevere et al. (2003) performed full-scale tests on realistic, rectangular and L-shaped residential structures. Results from these studies showed that light-frame roof diaphragms act relatively stiff compared to shear walls. Additionally, in-plane walls (parallel to applied lateral loads) are capable of sharing approximately 20 to 80 percent of their loads with other walls in the structure depending on the relative location and stiffness of the surrounding walls (Paevere et al. 2003). Data from these tests have also been used by a number of researchers to develop practical models for load path analysis.

Doudak (2005) developed a non-linear model of the Paevere et al. (2003) house, using a rigid element for the roof diaphragm. Individual sheathing nail connections were modeled using non-linear spring elements. The model was capable of predicting lateral load distributions to the walls, however, the level of detailing in the walls proved time consuming. Kasal (1992) and Collins et al. (2005) developed non-linear models of the Phillips et al. (1993) and Paevere et al. (2003) houses, respectively, also using rigid elements for the roof diaphragm. Unlike Doudak (2005), the in-plane stiffness of the shear walls was controlled using diagonal non-linear springs. This reduced the amount of time required for modeling; however, full-scale tests were necessary

to determine the non-linear stiffness of the springs and material properties for the structure. None of these models were used to examine uplift load paths. Shivarudrappa and Nielson (2011) modeled uplift load paths in light-frame roof systems. For increased accuracy, the models incorporated individual trusses, sheets of sheathing (modeled with individual nail connections) and semi-rigid roof-to-wall connections. Results from the model showed that the load distribution was affected by the location of gaps in the sheathing as well as the stiffness of the sheathing and connections.

Martin et al. (2011) developed a simple, linear model of a rectangular structure tested at one-third scale at the University of Florida. The model relied on material properties and wall stiffness properties readily available in industry standards. The in-plane stiffness of the walls was controlled by adjusting the shear modulus of the wall sheathing. The roof diaphragm was modeled as semi-rigid with individual trusses and sheathing, although gaps between individual sheets of sheathing were not included. Martin et al. (2011) found that the linear modeling methods were sufficient for predicting lateral load paths as well as uplift load paths through the structure when loaded within the elastic range. Additionally, the distribution of uplift loads was highly dependent on the orientation of the roof trusses. The modeling methods developed by Martin et al. (2011) were used in the current study to analyze lateral and uplift load paths in a more realistic light-frame house. A more detailed review of previous full-scale testing and modeling can be found in Pfretzschner (2012).

RESEARCH METHODS

The two main objectives of this study were to: (1) further develop and validate the practical, linear modeling methods of Martin et al. (2011) for a rectangular building, and (2) apply the modeling methods towards investigating uplift and lateral load paths in a realistic light-frame structure with complex geometry (L-shaped house). The modeling methods were developed using SAP2000 software (Computers and Structures, Inc. 2009). Additional details about the research methods can be found in Pfretzschner (2012).

Modeling Methods

Framing Members

Framing members, including wall studs, truss chords, etc., were modeled using SAP2000's frame element. The frame element was assigned the actual cross-section of each framing member. Multiple framing members located side by side, such as a "double stud" or "double top-plate," were modeled using a single frame element with a cross section equal to the sum of the individual cross sections of the framing members.

Isotropic material properties for the framing members were determined using longitudinal design properties listed in the AF&PA (2005a) *National Design Specification for Wood Construction* (NDS) based on wood species and grade. Adjustment factors for moisture content, incising, etc, were applied to the design properties as specified by the NDS (AF&PA 2005a).

Sheathing

Wall sheathing in the current study was modeled using SAP2000's layered shell element with plywood and gypsum wallboard (GWB) assigned as individual layers. Each shell element was modeled through the center of the wall studs with the sheathing layers displaced to either side of the wall. Roof and ceiling sheathing were also represented using the layered shell element; modeled through the centerline of the truss chords, with one layer of either plywood or GWB displaced accordingly.

Plywood layers were assigned orthotropic properties calculated using Nairn (2007) OSULaminates software. Plywood sheathing layers for the walls and roof were assigned in-plane and out-of-plane properties, respectively, based on their general behavior within the full building. GWB layers were assigned isotropic material properties listed by the Gypsum Association (2010).

In accordance with Martin et al. (2011), individual sheets of plywood and GWB were not modeled as separate elements. Instead, one continuous shell element was applied to each wall, ceiling and roof surface, and meshed into smaller elements for analysis. Although the effects of "gaps" between individual sheathing members were neglected, validation studies against full-scale tests showed that these methods were sufficient for portraying system behavior and load distribution.

Framing Connectivity

All framing connections were modeled as either simple "pinned" or "rigid" connections. Trusses were modeled with pinned connections at the ends of the webs and at the ridge. Rigid connections were used at the truss heels, and top and bottom chords were modeled as continuous members through the web connections. Truss-to-wall connections were modeled as rigid connections and were not coincident with the heel connections (Martin et al. 2011), however, in retrospect would be more accurately modeled as pins and rollers. Gable-end trusses were also rigidly connected to the gable-end walls.

All framing connections in the walls were modeled as pinned connections. This allowed for the stiffness of the walls to be controlled entirely by the sheathing properties. Shear wall stiffness is highly dependent on the spacing of the nail connections between the sheathing and framing members. As in Martin et al. (2011), the effects of edge nail spacing on wall stiffness were incorporated by adjusting the shear modulus, G_{12}, of the wall sheathing.

Sheathing G_{12} Adjustment Procedure

To account for the effects of sheathing edge nail spacing, the shear modulus, G_{12} of the sheathing was adjusted using a procedure similar to the "correlation procedure" used by Martin et al. (2011). The shear modulus of the sheathing was adjusted to account for the effects of edge nail spacing on overall wall stiffness rather than modeling individual nailed connections. The procedure in the current study was performed using a simple "*calibration model*" of a wall in SAP2000; with a specific length, rigid supports, no openings, and sheathed on one side only. Material properties were assigned to the sheathing using the previously described methods. G_{12}, of the sheathing was then altered until the deflection of the calibration model matched the predicted deflection calculated using Equation C4.3.2-2 from AF&PA (2005b) for a specific edge nail spacing and wall length.

Equation C4.3.2-2 is a three-term, linear equation used to predict deflections of wood-framed shear walls based on "framing bending deflection, panel shear deflection, deflection from nail slip, and deflection due to tie-down slip" (AF&PA 2005b). The effects of panel shear and nail slip are incorporated into an apparent stiffness term, G_a. Values for G_a are tabulated in AF&PA (2005b) based on sheathing material, framing lay-out and edge-nail spacing. Since rigid supports were used in the calibration model, the deflection due to tie-down slip was ignored in the three-term equation. The purpose of the calibration model was to determine the required

stiffness of the sheathing element. The effects of the anchor bolts and hold downs were incorporated later on, into the actual wall models used in the shear wall validation and full building models, by using linear springs with realistic stiffness properties.

Repeating this method for shear walls of various lengths revealed that the required G_{12} for a specific edge nail spacing varied approximately linearly with wall length. Thus, for a building with multiple wall lengths and uniform edge nail spacing, this procedure is only necessary for the shortest and longest walls in the building. Additionally, G_{12} for the plywood sheathing and GWB sheathing can be determined separately using the procedure above for a wall sheathed on one side and applied to the respective sides of a wall sheathed on two sides. This method is supported by Patton-Mallory et al. (1984), who found that the stiffness of a wall sheathed on two sides is equal to the sum of the stiffnesses of two walls sheathed on one side with the same materials.

Application of the sheathing adjustment procedure to the Paevere et al. (2003) house is shown in the following model validation procedure section.

Wall Anchorage

Anchor bolts and hold-downs were modeled using directional linear spring elements. Three springs were used for the anchor bolts: one oriented in the vertical, Z-direction (representing the axial stiffness of each bolt connection), and two oriented in the lateral, X- and Y- directions (representing the shear stiffness of each bolt connection). Hold-down devices were represented with only one spring oriented in the Z-direction.

The axial stiffness of the anchor bolts was assigned in accordance with Martin et al. (2011) based on full-scale tests performed by Seaders (2004). The full-scale tests incorporated the effects of bolt slip and wood crushing under the washers. The lateral stiffness of the anchor bolts was calculated using equations for the load slip modulus, γ, for dowel type connections in Section 10.3.6 of the NDS (AF&PA 2005a). Finally, the axial stiffness of the hold-down devices was determined from properties published by the manufacturer, Simpson Strong-Tie.

Model Validation Procedure

Similar to Martin et al. (2011), the modeling methods in this study were validated against full-scale tests. Sub-assembly models, including two-dimensional trusses, three- dimensional roof assemblies and two-dimensional shear walls, were validated against tests performed by

Wolfe et al. (1986), Wolfe and McCarthy (1989) and Dolan and Johnson (1996), respectively. Shear walls from Dolan and Johnson (1996) were anchored with both anchor bolts and hold-downs allowing for the simultaneous validation of anchorage and shear wall modeling methods. Details for the sub-assembly models are included in Pfretzschner (2012). The final validation study was performed using full-scale tests on a realistic L-shaped house from Paevere et al. (2003).

Paevere et al. (2003) House (Fig. 1)

Paevere et al. (2003) performed static, cyclic and destructive load tests on a full-scale, L-shaped house (Fig. 1). The house was designed to reflect a typical, North American "stick frame" house with a gable-style roof. Construction details for the L-shaped house can be found in Paevere et al. (2003) and Paevere (2002). Results from the static load tests were used to validate a model of the house.

Figure 1 shows the layout and framing used for the walls in the house, including six exterior shear walls (W1, W2, W4, W5, W7 and W9) and three interior non-load bearing walls (W3, W6 and W8). The exterior walls were 2.4 m (7.9 ft) tall. The interior walls were modeled 25 mm (1 in.) shorter than the exterior walls so that the trusses spanned the exterior walls only (Dr. Phillip Paevere, personal communication, June 25, 2012). W3 was connected to the trusses using non-structural slip connections to restrain the trusses laterally (Paevere 2002). These connections were modeled in SAP2000 using two-joint link elements, "fixed" in the direction parallel to the wall. Interior walls 6 and 8 were not connected to the trusses.

The gable roof was modeled as a semi-rigid diaphragm with 1.6-m- (5.2-ft-) tall, Fink trusses, spaced 0.6 m (2 ft) on center and oriented as shown in Figure 2, and plywood sheathing. Unsheathed Fink trusses were also used for the gable-end trusses. Framing members used for the truss chords and webs were 35x90 mm (1.4x3.5 in.) and 35x70 mm (1.4x2.8 in.), respectively. Details for the roof over-framing, where the two legs of the "L" meet above the garage, were not included in Paevere (2002) or Paevere et al. (2003). Therefore, over-framing in the model was assumed based on typical, North-American residential construction methods shown in Figure 2. It was modeled as a ridge-board with rafters. All framing members were assigned the same cross-sectional dimensions as the roof truss chords. All connections were modeled as pinned.

All framing members in the house were Australian radiata pine sawn lumber. Since radiata pine is not included in AF&PA (2005a), the MOE reported by Paevere (2002) of 10000

MPa (1450 ksi) was used for the frame elements in SAP2000. Sheathing consisted of 9.5-mm- (0.375-in.-) and 12.5-mm- (0.492-in.-) thick plywood on the walls and roof respectively, with 13-mm- (0.5-in.-) thick GWB interior lining on the walls and ceiling. All walls were fully sheathed on the interior with GWB. Exterior walls were fully sheathed on the outside with plywood with the exception of walls 5 and 9. The partial exterior sheathing used for walls 5 and 9 is shown in Figure 3.

Table 1 provides the material properties used to model the sheathing elements. Figure 4 shows the required G_{12} versus wall length for the plywood and GWB wall sheathing based on edge fastener spacing. The fasteners used for the plywood sheathing were equivalent to 6d common nails spaced at 152 mm (6 in.) along the edges. The GWB fasteners were equivalent to No. 6 drywall screws spaced 305 mm (12 in.) along the edges. The maximum fastener spacing listed in AF&PA (2005b) of 203 mm (8 in.) for GWB sheathing was used to determine values of G_{12} for the GWB in the model.

The walls were anchored with 12.7 mm (0.5 in.) diameter anchor bolts, only (no hold-downs were used). Vertical and lateral springs used to represent the axial and shear behavior of the bolt connections were assigned a stiffness of 6.1 kN/mm (35 kip/in) and 16.7 kN/mm (95.5 kip/in), respectively. Stiffness properties were determined from Seaders (2004) and AF&PA (2005a) as explained in the modeling methods. Each anchor bolt in the full-scale house was connected to a load cell capable of measuring lateral and vertical reactions. Reactions at the anchor bolts in the model were validated against reactions from Paevere et al. (2003) for 15 static load tests consisting of one gravity load test and 14 lateral, concentrated load tests. Table 2 lists the material densities used to model the self weight (gravity loads) of the house. A complete list of lateral load cases can be found in either Paevere (2002) or Pfretzschner (2012).

Load Path Investigations

After the modeling methods were validated, variations of the Paevere et al. (2003) house were created and used to perform load path investigations for uniform uplift pressures and ASCE 7-05 design wind loads. All structures used in the investigations were modeled based on the materials and construction methods used by Paevere et al. (2003) with the following exceptions: (1) Gable-end overhang framing was changed to “out-looker” or “out-rigger” style framing commonly used in North America (Martin et al. 2011). (2) Gable-end trusses were changed from Fink trusses to more common, non-structural gable-end trusses. Modified gable-end

framing is shown in Figure 5. (3) The exterior was fully sheathed with plywood, including the gable-end trusses. The shell element used to model the sheathing on the gable-end truss was not connected to the shell element used for sheathing on the gable-end wall. (4) Simpson Strong-Tie HDU2 hold-downs, modeled with an axial stiffness of 6.1 kN/mm (35 kip/in), were added to the exterior walls at the ends and at either side of door openings.

For each load path investigation, index buildings were created as a baseline for load path comparisons. The index buildings were then altered systematically to analyze the effects of geometric variations (wall openings and re-entrant corners) and gable-end retrofits on uplift and lateral load paths. Detailed descriptions of the structures used in the load path investigations can be found in Pfretzschner (2012).

Uniform Uplift Investigation

As an extension of Martin et al. (2011), the effects of re-entrant corners and large wall openings were explored under a uniform uplift pressure of 2.4 kPa (50 psf) acting normal to the surface of the roof.

Two simple index buildings were used for the uplift investigation: a *rectangular index building* and an *L-shaped index building*. The L-shaped index building had the same plan geometry as the Paevere et al. (2003) house; with the modifications described previously, no interior walls, no wall openings and no GWB lining. The rectangular index building was then created by removing the short leg of the "L" and extending wall 2. Note that the wall designations used by Paevere et al. (2003) (shown in Figure 1) were maintained throughout both load path investigations. Similar to Martin et al (2011), the self-weight of the buildings was not included in order to analyze load paths due to uplift pressures, only. Reactions at the anchor bolts and hold-downs of the L-shaped index building were compared to the rectangular building to analyze the effects of the re-entrant corner.

The redistribution of load paths due to large wall openings was also explored in this investigation. Martin et al. (2011) analyzed the effects of wall openings on uplift load paths in a simple rectangular building. In the current study, the effects of large, 3.2-m- (10.5-ft-) long, wall openings in the L-shaped index building were explored. Wall openings were added to the building one at a time in the following locations, representing scenarios that were not previously explored by Martin et al. (2011): wall 2 adjacent to the re-entrant corner, wall 4 opposite the re-entrant corner, wall 9 centered under the gable end, and wall 9 opposite the re-entrant corner.

Due to the configuration of the roof, wall 9 represents both a gable-end wall and a side wall, with trusses running both parallel and perpendicular to the wall.

Wind Load Investigation

The second load path investigation explored load paths in a more realistic house with applied ASCE 7-05 design wind loads. Design loads were calculated using the Main Wind Force Resisting System, MWFRS, method 2 (ASCE 2005). Although ASCE 7-05 MWFRS codified pressures are intended for buildings with regular plan geometry, a method for adapting the pressures to buildings with re-entrant corners is given in Mehta and Coulbourne (2010). This methodology was adopted for the current study. Additional methods of determining design wind loads for irregular buildings are discussed in Pfretzschner (2012).

Three wind directions were considered with design loads calculated based on ASCE 7-05 Load Cases 1 and 3 as shown in Figure 6. Load Case 1 includes all windward, leeward, sidewall and "roof parallel to wind" pressures indicated by ASCE 7-05 Figure 6-6. Load Case 3 is meant to simulate diagonal winds by combining leeward and windward pressures for X and Y winds acting simultaneously at 75% of their full design value (Mehta and Coulbourne 2010). Parameters for the design wind loads were selected in accordance with Martin et al. (2011) including: a basic wind speed of 209 km/h (130 mph), a topographic factor, K_{zt}, of 1.0 and exposure category, B. The building was assumed to be a low-rise, enclosed building with occupancy category II, and an importance factor of 1.0. Positive internal pressure was used to produce "worst-case" uplift scenarios.

The index structure for this investigation was a realistic *L-shaped index house*, different from the L-shaped index building, representing the Paevere et al. (2003) house with the gable-end framing, sheathing and hold-down modifications described previously. The L-shaped index house was then altered to investigate the effects of (1) the addition of gable-end retrofits at every gable-end stud, and (2) the effects of increasing the size of the re-entrant corner. The gable end retrofits were modeled based on the C-shaped, gable-end retrofit recently adopted into the 2010 Florida Building Code (ICC 2011). An additional stud was added at each vertical web in the gable-end trusses, with the strong axis oriented perpendicular to the wall (forming an "L") to reinforce the webs against out-of-plane winds. Note that ICC (2011) actually only requires the gable-end retrofits at studs exceeding 3 ft in length. However, the purpose in adding the retrofits was to examine any torsion in the building and not the effectiveness of the retrofit itself. The

study shows that even with retrofits at every stud there is no additional torsion in the building. Additionally, horizontal braces were added to help transfer load from the gable-end wall into the roof and ceiling diaphragm. Additional details about the retrofit can be found in ICC (2011). Figure 7 shows one of the C-shaped retrofits in the model, added at every gable-end stud. Connections between the retrofit studs and horizontal braces were accomplished with steel L-straps and compression blocks, and assumed to be rigidly connected in the model because of the overall configuration of the connection. No physical testing results are available, so it is possible that a pinned connection is more appropriate.

The effects of the re-entrant corner were explored by altering the short leg of the *L*-shaped index house to create three different sized re-entrant corners: *small*, *medium*, and *large*. For the small and medium re-entrant corners, the leg was shortened and lengthened by 2.4 m (7.9 ft) respectively. The large re-entrant corner was created by extending the leg so that the dimensions of the re-entrant corner had a 1:1 ratio. Wind loads for the re-entrant corner variations were adjusted accordingly based on the dimensions of the house.

RESULTS AND DISCUSSION

Model Validation

Sub-Assemblies

Sub-assembly models were used to validate the applicability of previously described modeling methods in predicting two- and three-dimensional system behavior. Two-dimensional models of individual trusses validated the use of ideal pinned and rigid connections between truss chords and webs. Three-dimensional models of roof assemblies validated the use of the layered shell element for modeling plywood sheathing. The roof assembly models were capable of predicting load sharing and relative truss deflection in roofs with variable truss stiffness. Finally, models of two-dimensional shear walls validated methods for incorporating the effects of sheathing edge-nail spacing, wall openings and wall anchorage on shear wall stiffness. Full details and results for the sub-assembly validation studies are included in Pfretzschner (2012).

Paevere et al. (2003) House

The full-scale L-shaped house, tested by Paevere et al. (2003), was used to validate the ability of the model to predict load sharing between walls connected by the roof diaphragm in a

realistic house. Reactions at the anchor bolts in the model were compared against reactions in the full-scale house for 15 static load cases. It should be emphasized that the load distributions here and for full building models are examined at the foundation level rather than at the roof-to-wall connections. The variation may be less at the foundation level as the loads distribute through the walls. The first static load case included gravity loads only to determine the self-weight of the house. Paevere et al. (2003) measured a self-weight of 50.8 kN (11.4 kips), which was only 9% smaller than the self-weight of the model: 55.7 kN (12.5 kips) and this was considered to be close enough.

The remaining 14 load cases consisted of concentrated lateral loads applied at various locations along the top chords of walls 4 and 5, and at various angles at the roof ridge directly above wall 5. The distribution of lateral loads to the in-plane walls of the model was compared to reactions from Paevere et al. (2003). Figure 8, for example, compares the load distributions from the test house and the model for Load Case 4. Results from all 14 lateral load cases can be found in Pfretzschner (2012). Overall, the model proved capable of predicting the overall trends in load distributions (Figure 8) to the in-plane walls. Reactions at the walls carrying the maximum in-plane load were predicted within 20% error on average. For example, the largest load in Figure 8 occurred at wall 3 and was accurate to about 17%. This is similar to the level of accuracy reported by Doudak (2005) for static loading and elastic behavior of the structure.

Uniform Uplift Investigation

The vertical reactions and changes in reaction at the anchor bolts and hold-downs of the models used in the uplift investigation were recorded and plotted in "bubble" plots. Each bubble represented an anchor bolt or hold-down while the size of the bubble represented the magnitude of either the uplift reaction or change in reaction at that anchorage device. The locations of the hold-downs were designated with an x. Detailed reaction plots for all model variations can be found in Pfretzschner (2012).

Rectangular vs. L-Shaped Buildings

To analyze the effects of re-entrant corners, the uplift reactions for the rectangular and L-shaped index buildings were plotted in Figure 9. Uplift reactions in the rectangular building were symmetrical with a maximum reaction of 11.0 kN (2.5 kips), which is 0.17 kN/m^2 of floor area, and occurring at the anchor bolts at the center of the side walls (walls 2 and 4). Since the

roof trusses spanned between the side walls, the majority of the load applied to the roof was directed into the side walls rather than the gable-end walls. The maximum uplift reaction in the L-shaped index building, on the other hand, was 14.7 kN (3.3 kips), which is 0.16 kN/m^2 of floor area, and occurring at the hold-down directly under the re-entrant corner. In this case, the uplift loads that would have been transferred to the west side of wall 2 in the rectangular building, were instead transferred to the garage beam in the L-shaped building (shown in Figure 1b). The garage beam then directed the loads to the re-entrant corner and wall 9 opposite the re-entrant corner, causing load concentrations at these locations. Uplift load concentrations also occurred at anchor bolts under wall 4, directly opposite the re-entrant corner. The flow of loads in the L-shaped index building is illustrated by the arrows in Figure 9. Note that trusses span perpendicularly from the re-entrant corner to wall 4 at this location. The load distribution to wall 5, parallel to the trusses, was not affected by the addition of the re-entrant corner. This suggests that the re-distribution of uplift loads due to a re-entrant corner is dependent on the orientation of the roof trusses with respect to the walls. A similar observation was noted by Martin et al. (2011) when investigating the effects of wall openings. Future research should examine the effects of re-entrant corners in buildings with different truss orientations.

Effects of Wall Openings

Martin et al. (2011) explored the effects of large wall openings placed in the gable-end walls and side walls of a rectangular building under uniform uplift pressure. The current study examined openings in an L-shaped building with a re-entrant corner and trusses oriented in two orthogonal directions. Similar to Martin et al. (2011), the opening centered under the gable-end portion (North end) of wall 9 caused relatively localized effects, increasing uplift loads in the side wall portion (South end) of wall 9, and having negligible effects on walls on the opposite side of the building. The openings placed in the side walls, on the other hand, had more global effects on uplift reactions throughout the building. Figure 10 shows the change in uplift reactions due to openings in the two different side walls: wall 4 (opposite the re-entrant corner) and wall 2 (adjacent to the re-entrant corner). The increase of 60% in Figure 10 is compared to the uplift reaction at the same location along wall 2 in the L-shaped index building without wall openings in Figure 9 (not labeled). As expected, uplift loads at the location of the openings were re-directed through the headers to either side of the doors, causing load concentrations at the hold-downs directly under the door jams. The largest load concentrations were seen on the side

of the opening in wall 2, closest to the re-entrant corner. Uplift reactions at this point increased by 60 percent over the reactions seen in the building without openings. Comparatively, the opening in wall 4 caused less than a 30 percent increase in uplift loads at either side of the opening. The larger load concentration at the opening in wall 2 was likely due to the uplift load concentrations in wall 2 from the re-entrant corner itself.

As in Martin et al. (2011), openings placed in the side walls in this investigation also caused uplift load concentrations in the remaining side walls. Examining the truss orientation in the building shows that uplift loads at these points of concentration were clearly transferred from either side of the wall opening by the roof trusses. In the case of the opening in wall 4, for example, uplift loads were transferred from the east side of the wall opening, through the north-south trusses, to the opposite side wall (wall 2). Uplift loads were also transferred from the west side of the opening, through the north-south trusses to the garage beam shown in Figure 1(b), and redirected through the garage beam and the east-west trusses to wall 9 (adjacent to wall 4). Similar system behavior was seen for the opening in wall 2 as shown in Figure 10, and for other side wall openings included in Pfretzschner (2012). This strongly supports findings from Martin et al. (2011) that the effects of openings on uplift load distribution are dependent on the relative truss orientation with respect to the walls. The effects of openings in walls perpendicular to the trusses were shared by other walls in the building spanned by the same trusses, while the effects of openings in walls parallel to the trusses were more isolated.

Finally, Martin et al. (2011) reported that the addition of an opening to any wall resulted in a decrease in the total load carried by the wall. In the current study, the opening in wall 2 also caused a decrease in the total load carried by the wall of up to 20 percent. The opening placed in wall 4, however, caused a 0.2 percent increase in the amount of total uplift load carried by the wall. It is likely that this small increase was due to the effects of the re-entrant corner.

Wind Load Investigation

Uplift reactions for each of the model variations in the wind load investigation were also plotted in bubble graphs and included in Pfretzschner (2012). Figure 11 shows the uplift reactions at the anchor bolts and hold-downs in the L-shaped index house for each wind load case. In all cases, uplift load concentrations were seen at the hold-downs located under the corners of the house, as well as on either side of the door openings. In addition, to determine whether the large uplift reactions at the west gable-end were due to the geometry of the building

or the selected load cases, a fourth load case for east to west winds was added. This demonstrated that uplift reactions at the east gable end under the east to west wind loads were of similar magnitude to the reactions at the west gable-end under west to east wind loads.

Lateral load distributions to the walls parallel to the wind loads, for each model, were also plotted (Figure 12) and used to support the findings described below. For the southeast-northwest load case, lateral load distributions to both the N-S and E-W walls were plotted. Note that walls 6, 7 and 8 (shown individually in Figure 1) were grouped together here to simplify data presentation.

Addition of Gable-End Retrofits

Due to the number of gable-end failures seen in the aftermath of hurricanes, the 2010 Florida Building Code recently adopted a C-shaped gable-end retrofit for existing buildings (ICC 2011). Full-scale tests performed on gable-end sections (comprised of four Fink trusses and a gable-end wall) by Suksawang and Mirmiran (2009) showed that the retrofit sufficiently increased the strength of the gable-ends. However, questions remained about whether load redistribution due to the retrofit could cause additional torsion within a full building (beyond the original design). To address this question, C-shaped retrofits were modeled at every gable-end stud within the L-shaped index house used in this investigation.

The distribution of lateral loads and top plate deflections of the walls were then analyzed under ASCE 7-05 design wind loads for signs of torsion. For all wind load cases, the addition of the gable-end retrofits to the L-shaped index house caused negligible changes in lateral reactions under the walls parallel to the wind loads. Changes in deflections were equally small, within 0.1 mm (0.004 in), and showed no signs of additional torsion. These results were based on the three ASCE 7-05 load cases shown in Figure 6 only. Additionally, alternative retrofits recommended by the 2010 Florida Building Code for buildings with pre-existing obstacles were not explored in this investigation.

Effects of Re-Entrant Corner Dimensions

Figure 12 shows the lateral load distributions to the walls parallel to the wind loads and displaced shapes of the exterior wall top-plates for each wind load case. For north to south (N-S) design wind loads, the displaced shape of the top-chords for each model variation showed little to no torsion due to the increasing size of the re-entrant corner. As walls 7 and 9 were extended, lateral loads carried by the outer walls running N-S (walls 5 and 9) were re-distributed to the

inner N-S walls 6, 7 and 8. The percent of N-S loads carried by these central walls increased by 14 percent; while the percent of N-S loads carried by the outer walls, walls 5 and 9, decreased by 7 and 3 percent, respectively.

In the case of west to east (W-E) wind loads, the displaced shape of the top chords clearly showed increasing degrees of torsion as the size of the re-entrant corner increased. Although the relative distribution of these loads to each of the W-E walls changed by less than 5 percent, increasing the length of the southern end of wall 9 (perpendicular to the wind) increased the total amount of W-E wind load on the house. As a result, the relative in-plane deflections of southern walls 1 and 2 as compared to northern walls 3 and 4 increased dramatically. This can be attributed to the fact that walls 1 and 2 were significantly less stiff than walls 3 and 4, due to the shorter lengths and relatively large opening to surface-area ratios of walls 1 and 2. This asymmetry in relative stiffness between the north and south sides of the house caused torsion to occur with increasing loads in the W-E direction. Wind loads applied diagonally, southeast to northwest (SE-NW), into the re-entrant corner also caused increasing amounts of torsion as the size of the re-entrant corner increased. For all load cases, the effects of increasing the size of the re-entrant corner were dependent on the relative stiffness and location of the walls, as well as the orientation of the wind loads. Additionally, the displaced shapes of the top plates in Figure 12 show a combination of torsional behavior and in-plane displacements characteristic of a semi-rigid diaphragm.

The results of this study imply that balancing the stiffness of the walls along each of the major axes of the house may reduce torsion due to large re-entrant corners. In an effort to reduce torsion in the model with the largest re-entrant corner, the stiffnesses of walls 1 and 2 were increased by assuming realistic changes in the construction of the walls: (1) blocking was added to the walls, (2) the edge fastener spacing for the GWB was decreased to 102mm (4 in), (3) the nails used for the plywood were upgraded from 6d to 8d common nails and (4) the edge nail spacing for the plywood was decreased to 51 mm (2 in). Based on these assumptions, new values of G_{12} for the GWB and plywood sheathing on walls 1 and 2 were calculated using the adjustment procedure described in the modeling methods section. Figure 13 shows the deflected shapes of the original model and the model with increased stiffnesses in walls 1 and 2 for the W-E and SE-NW wind loads. In both cases, increasing the stiffnesses of walls on the south side of the house slightly decreased the amount of torsion seen in the deflected shape of the top chords.

CONCLUSIONS

Based on the validation studies, the simplified linear modeling methods created by Martin et al. (2011), and further developed in this study, were capable of predicting uplift and lateral load paths in a light-frame, wood residential structure with complex, realistic plan geometry. This conclusion is strictly for loading conditions within the elastic range of the structure. The modeling methods used in this study cannot be applied for inelastic or failure analysis.

Using the validated modeling methods, two different load path investigations were performed using uniform uplift pressures and ASCE 7-05 design wind loads. The following conclusions were drawn based on results from the load path investigations:

1. The addition of a re-entrant corner in a low-rise structure, under uniform uplift pressure, caused load concentrations at the re-entrant corner as well as in either wall directly opposite the re-entrant corner; depending on the truss orientation. For example, when the re-entrant corner was extended by 2.4 m, making the dimensions of the corner a 1:1 ratio, loads carried by internal walls parallel to the wind increased by 14 % while outer walls parallel to the wind decreased by 3-7 %.
2. The addition of wall openings in a low-rise structure under uniform uplift pressure caused load concentrations on either side of the openings. Uplift loads at these points of concentration were further distributed to the remaining walls by the roof trusses. The largest load concentrations occurred when an opening was placed in a side wall, directly adjacent to the re-entrant corner. Openings in walls parallel to the trusses had the least effect on uplift reactions in the remaining walls. Thus, homes with large openings such as garage doors in the side walls are more vulnerable to uplift loads than ones with the openings in the gable-end walls.
3. ASCE 7-05 Main Wind Force Resisting System (MWFRS) design wind loads caused uplift load concentrations at the hold-downs placed under the door jams and the corners of the L-shaped house.
4. There was no evidence that the gable-end retrofit adopted by the 2010 Florida Building Code caused additional torsion in the L-shaped house when loaded with ASCE 7-05 MWFRS design wind loads.

5. The effects of increasing the size of the re-entrant corner in an L-shaped house, under ASCE 7-05 MWFRS design wind loads, were dependent on the location and relative stiffness of the in-plane walls, as well as the assumed direction of the wind.

ACKNOWLEDGMENTS

Previous research contributions from Kenneth Martin, Dr. Phillip Paevere and Dr. Bohumil Kasal were greatly appreciated, as well as funding from the Oregon State University Center for Wood Utilization Research.

REFERENCES

AF&PA (2005a). *National Design Specification for Wood Construction (NDS).* ANSI/AF&PA NDS-2005. Washington, DC.

AF&PA (2005b). *Special Design Provisions for Wind and Seismic.* ANSI/AF&PA NDS-2005. Washington, DC.

ASCE – American Society of Civil Engineers. (2005). *ASCE/SEI 7-05 Minimum Design Loads for Buildings and Other Structures.* New York, NY.

Computers and Structures, Inc. (2009). *CSI Analysis Reference Manual: For SAP2000, ETABS and SAFE*. Berkeley, CA.

Collins, M., Kasal, B., Paevere, P. and Foliente, G. C. (2005). "Three-Dimensional Model of Light Frame Wood Buildings. II: Experimental Investigation and Validation of Analytical Model." *Journal of Structural Engineering*, 131(4), 676-683.

Dolan, J.D. and Johnson, A.C. (1996) "Monotonic Tests of Long Shear Walls with Openings." Virginia Polytechnic Institute and State University Timber Engineering Report TE-1996-001, Blacksburg, VA.

Doudak, G. (2005). "Field Determination and Modeling of Load Paths in Wood Light-Frame Structures." PhD. Thesis, McGill University, Montreal, Quebec.

EWPPA - Engineered Wood Products Association of Australia (2009). "Structural Plywood and LVL Design Manual." *EWPAA Design Guides*, <http://www.ed.ewp.asn.au:85/Library/document_List.aspx?type=Design> (July 19, 2012).

Gypsum Association (2010). "Gypsum Board Typical Mechanical and Physical Properties." Gypsum Association (GA 235-10), Hyattsville, MD.

Holmes, J.D., (2001). *Wind Loading of Structures.* Spon Press, New York, NY.

ICC (2011). *Florida Building Code 2010 – Residential.* International Code Council, Inc. Country Club Hills, IL.

Kasal, B. (1992) "A Nonlinear Three-Dimensional Finite-Element Model of a Light-Frame Wood Structure." Ph.D. Diss., Oregon State University, Corvallis, Oregon.

Martin, K. (2010). "Evaluation of System Effects and Structural Load Paths in a Wood Framed Structure." M.S. Thesis, Oregon State University, Corvallis, OR.

Martin, K.G., Gupta, R., Prevatt, D.O., Datin, P.L., van de Lindt, G.W., (2011). "Modeling System Effects and Structural Load Paths in a Wood-Framed Structure." *Journal of Architectural Engineering*. 17, 134-143.

Mehta, K.C. and Coulbourne, W.L. (2010). *Wind Loads: Guide to the Wind Load Provisions of ASCE 7-05*. ASCE Press, Reston, VA.

Nairn, J. (2007). *OSULaminates – Java Application for Laminated Theory Analysis, Version 2.1.* Available at: < http://www.cof.orst.edu/cof/wse/faculty/Nairn/OSU Laminates.html> (July 31 2012).

Paevere, P. (2002). "Full-Scale Testing, Modeling and Analysis of Light-Frame Structures Under Lateral Loading." Ph.D. Diss., The University of Melbourne, Victoria, Australia.

Paevere, P., Foliente, A.M., and Kasal, B. (2003). "Load-Sharing and Redistribution in a One-Story Woodframe Building." *Journal of Structural Engineering*, 129 (9), 1275-1284.

Patton-Mallory, M., Gutkowski, R.M., and Solstis, L.A. (1984). "Racking Performance of Light-Frame Walls Sheathed on Two Sides." FPL-448. Forest Products Laboratory, Madison, WI.

Pfretzschner, K.S. (2012). "Practical Modeling for Load Paths in a Realistic, Light-Frame Wood House." M.S Thesis, Oregon State University, Corvallis, OR.

Phillips, T., Itani, R., and McLean, D. (1993). "Lateral Load Sharing by Diaphragms in Wood-Framed Buildings." *Journal of Structural Engineering, 119(5), 1556-1571.*

Prevatt, D.O., Roueche, D.B., van de Lindt, J.W., Pei, S., Dao, T., Coulbourne, W., Graettinger, A.J., Gupta, R., and Grau, D. (2012). "Building Damage Observations and EF Classifications from the Tuscaloosa, AL and Joplin, MO Tornadoes." Structures Congress 2012, ASCE 2012, 999-1010.

Seaders, P. (2004). "Performance of Partially and Fully Anchored Wood Frame Shear Walls Under Monotonic, Cyclic and Earthquake Loads." M.S. Thesis, Oregon State University, Corvallis, OR.

Shivarudrappa, R., Nielson, B.G. (2011) "Sensitivity of load distribution in light-framed wood roof systems due to typical modeling parameters." *Journal of Performance of Constructed Facilities*, Accepted Manuscript.

Suksawang, N. and Mirmiran, A., "Hurricane Loss Reduction for Housing in Florida: Performance of Gable End Wall Bracing Retrofit for Hurricane Protection, Phase II" Florida International University < http://www.ihrc.fiu.edu/lwer/docs/ Year%209_Section4_GableEndBracing_RCMP08-09.pdf> (July 22, 2012).

van de Lindt, J.W., Graettinger, A., Gupta, R., Skaggs, T., Pryor, S., and Fridley, K.J., (2007). "Performance of Wood-Frame Structures during Hurricane Katrina." *Journal of Performance of Constructed Facilities*, 21(2), 108-116.

Wolfe, R.W., and McCarthy, M. (1989). "Structural Performance of Light Frame Roof Assemblies – I. Truss Assemblies with High Truss Stiffness Variability" FPL-RP-492. Forest Products Laboratory, Madison, WI.

Wolfe, R.W., Percival, D.H., and Moody, R.C. (1986). "Strength and Stiffness of Light Framed Sloped Trusses." FPL-RP-471. Forest Products Laboratory, Madison, WI.

Manuscript Tables

Table 1: Sheathing Material Properties

Material	Properties	Source
Plywood Sheathing (Roof)	E_1 = 8280 MPa (1201 ksi) E_2 = 2393 MPa (347 ksi) U_{12} = 0.011 G_{12} = 482 MPa (70 ksi)	*OSULaminates (Nairn 2007) (Flexural Properties)*
Plywood Sheathing (Walls)	E_1 = 7017 MPa (1018 ksi) E_2 = 3657 MPa (530 ksi) U_{12} = 0.016	*OSULaminates (Nairn 2007) (In-Plane Properties)*
Gypsum Wallboard (Walls and Ceiling)	E_1 = 1820 MPa (264 ksi) E_1 = 1820 MPa (264 ksi) U_{12} = 0.3	*Gypsum Association (2010)*

Table 2: Material Densities used for Building Self-Weight

Material	Density kg/m^3 (pcf)	Source
Framing Members	550 (1.07)	*Paevere (2002)*
Plywood	600 (1.16)	*EWPAA (2009)*
GWB	772 (1.50)	*Gypsum Association (2010)*

Manuscript Figures

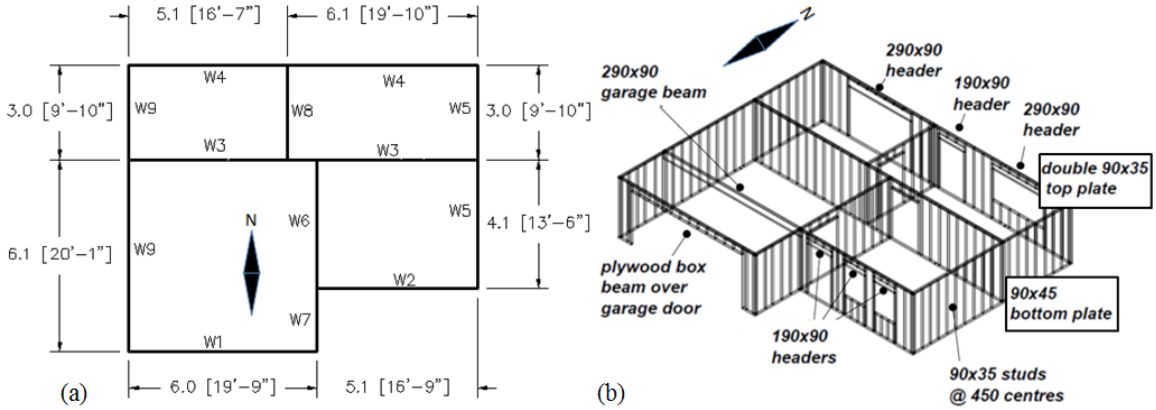

Figure 1: (a) Floor Plan with Centerline Dimensions [m (ft-in)] and Wall Designation, (b) Wall framing (mm) (Paevere 2002)

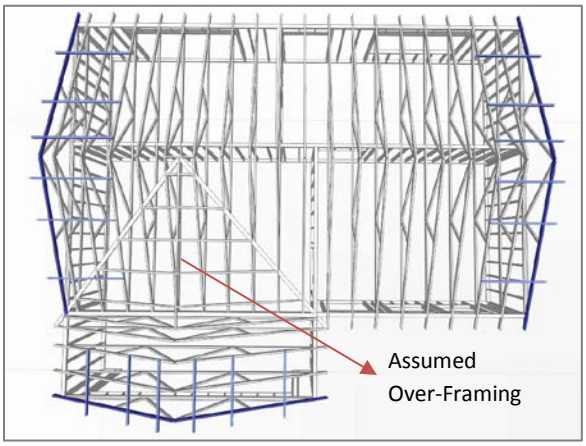

Figure 2: Truss Orientation and Gable-End Framing

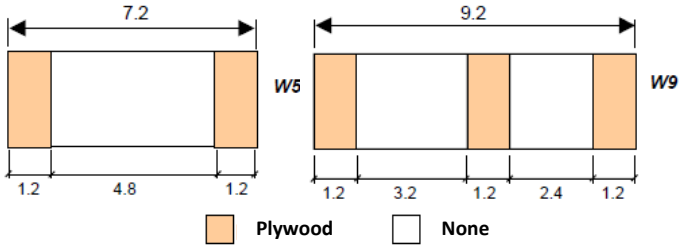

Figure 3: Plywood Sheathing on Exterior of Walls 5 and 9 (Paevere et al. 2003)

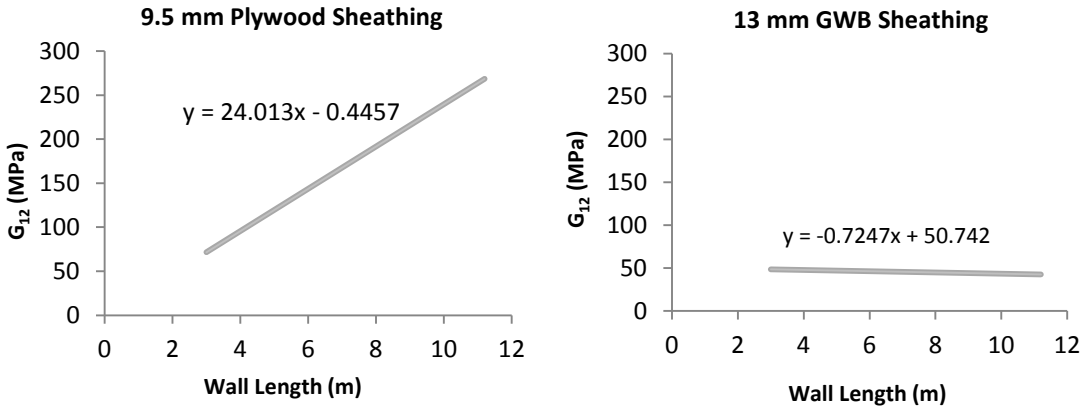

Figure 4: G_{12} vs. Wall Length for Plywood and GWB Wall Sheathing

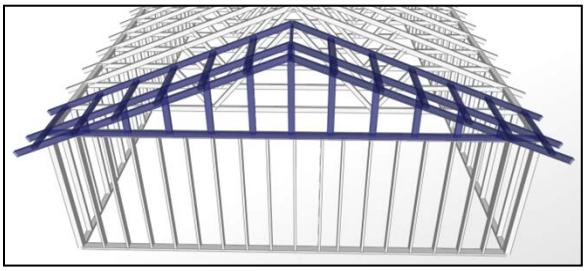

Figure 5: Modified Gable-End Framing for Load Path Investigations

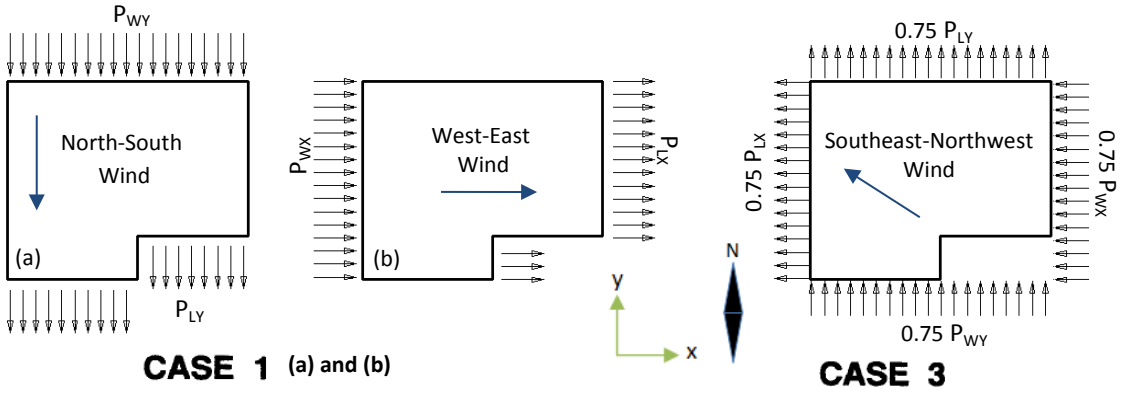

Figure 6: Wind Directions and ASCE 7-05 Load Cases

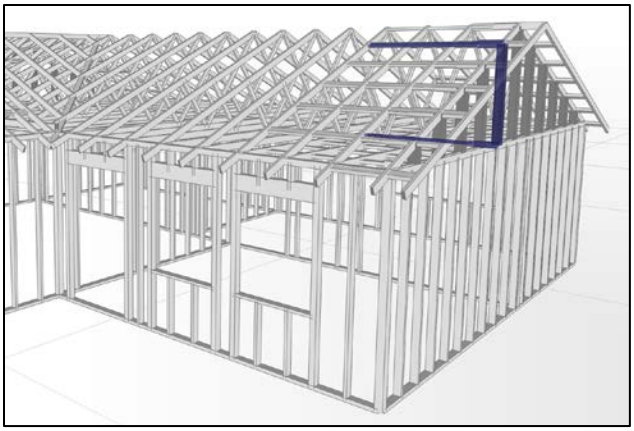

Figure 7: Example C-Shaped Gable-End Retrofit at Gable-End Stud

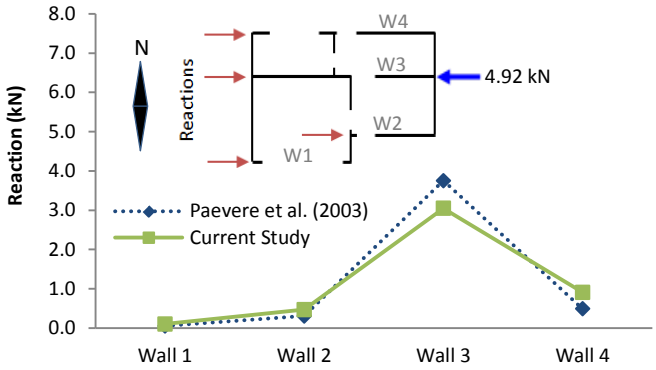

Figure 8: Load Distribution Plot for Paevere et al. (2003) Load Case 4

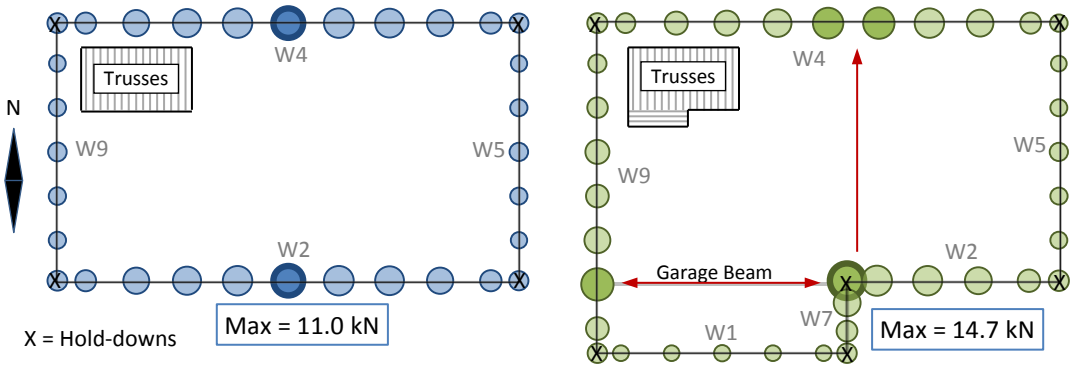

Figure 9: Uplift Reactions for Rectangular (Left) and L-shaped (Right) Index Buildings

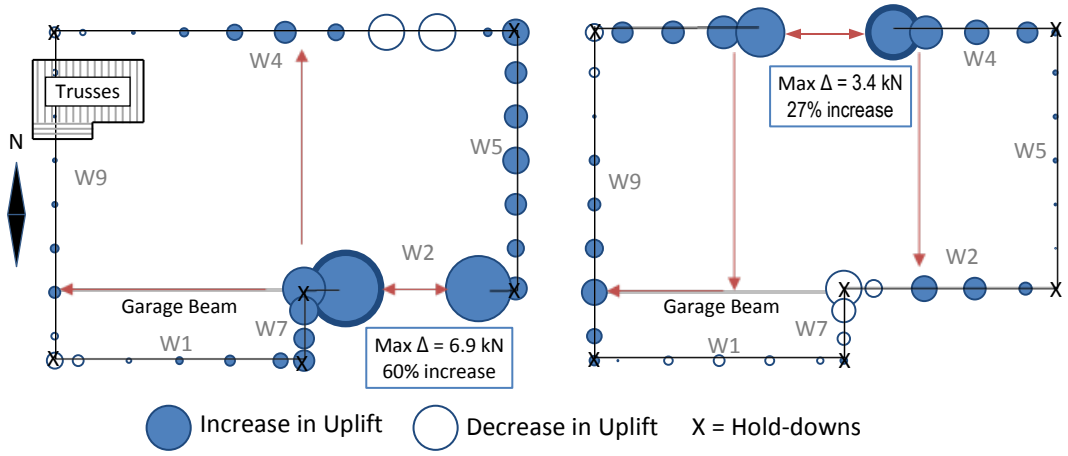

Figure 10: Change in Uplift Reactions (Magnified 4x) due to Openings in Wall 2 (Left) and Wall 4 (Right) – arrows represent load paths

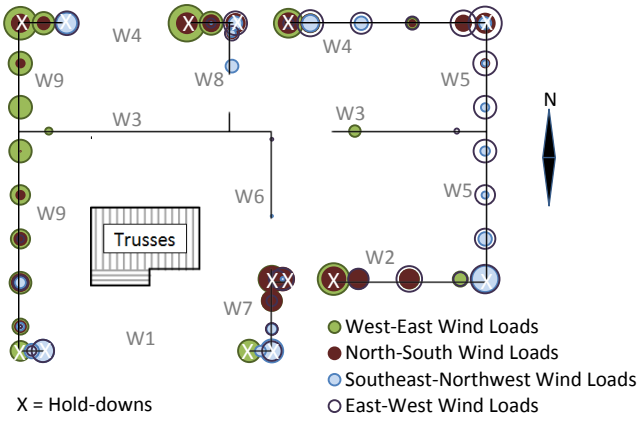

Figure 11: Uplift Reactions in L-Shaped Index House

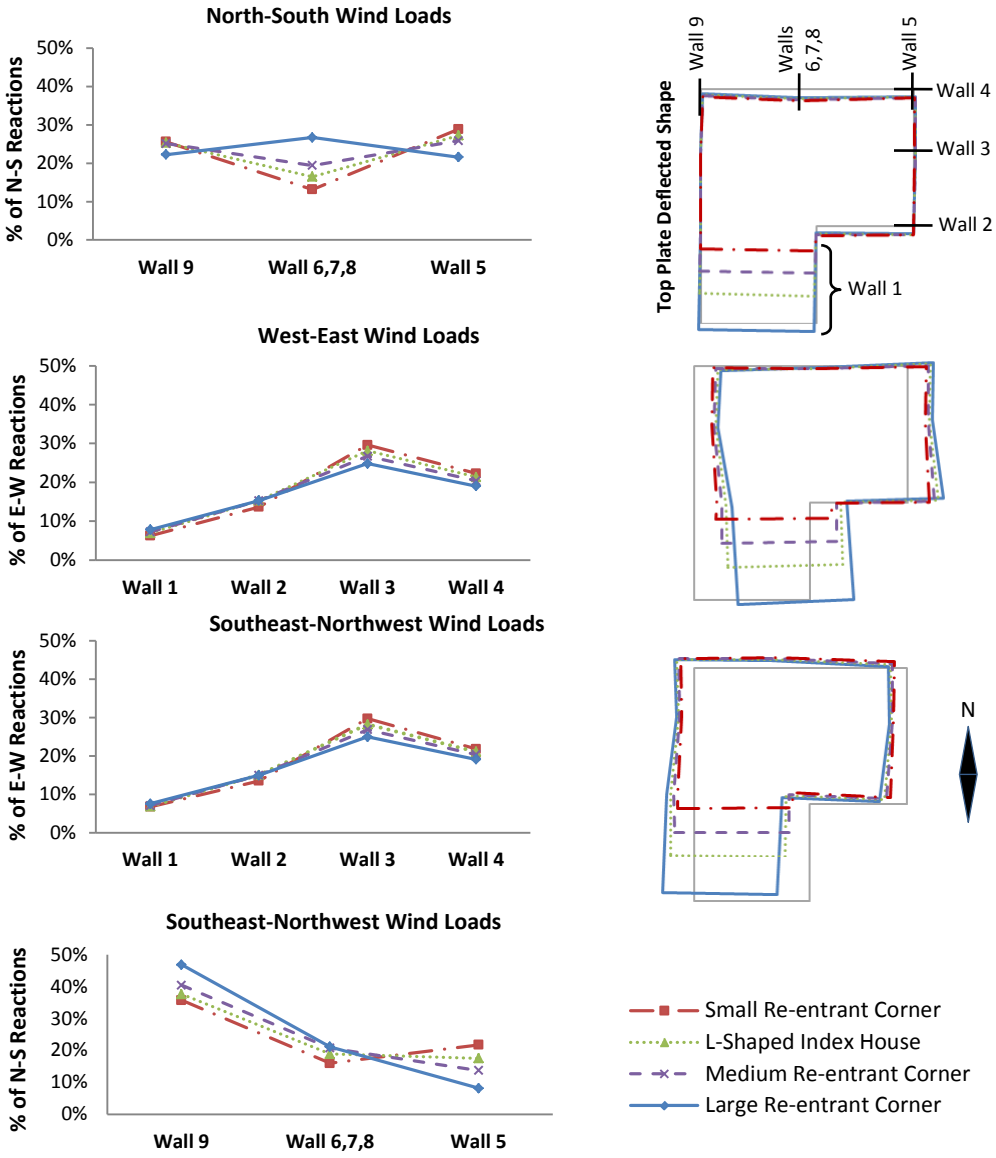

Figure 12: Lateral Load Distribution and Top Plate Deflected Shapes for Re-Entrant Corner Variations

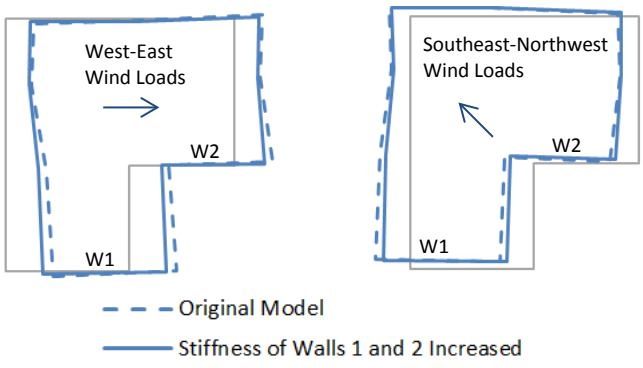

Figure 13: Displaced Shape of Large Re-Entrant Corner Building with Increased Stiffness in Walls 1 and 2